12th International Symposium on Turbulence and Shear Flow Phenomena (TSFP12)
Osaka, Japan (Online), July 19-22, 2022

I UNSTABLE NATURAL CONVECTION IN A VERTICAL CHANNEL WITH HOT-COLD WALL CONFIGURATION

ChungGang Li
Department of Computational Science
Kobe University
1-1 Rokkodai, Nada-ku, Kobe 657-8501, Japan
cgli@aquamarine.kobe-u.ac.jp

Makoto Tsubokura
Department of Computational Science
Kobe University
1-1 Rokkodai, Nada-ku, Kobe 657-8501, Japan
tsubo@tiger.kobe-u.ac.jp

ABSTRACT

The unstable phenomena induced by the natural convection in an open-ended vertical channel with a hot-cold wall configuration are investigated. The compressible solver combining absorbing and non-reflecting boundary conditions for extremely low Mach numbers is applied to eliminate the problem of requiring a priori knowledge of the flow rate. It is found that the existing empirical experience for the natural convection in a vertical channel cannot be applied to the current configuration. In order to better reflect the underlying physics, the turbulent behavior near the wall is investigated and the result shows that Grossmann-Lohse (GL) theory, originally proposed of horizontal (Rayleigh-Benard) convection, can be applied to describe the current flow behavior. From the correlation between the Rayleigh number and Nusselt number, it can be estimated that this kind of unstable phenomenon can enhance the heat transfer by around 10%.

Introduction

The natural convection in a vertical channel with hot-cold walls is very common to see in our daily life such as a wall-mounted-panel heater. Differently from one of the most well-known cases, the natural convection in an enclosure, how to well conditionally assign the boundary condition at inlet and outlet is a challenging topic. Especially, due to the different direction of the buoyancy force in a hot-cold wall configuration, the opposite velocities located on the same boundary for both upper and lower apertures in the channel increases the difficulty of performing the simulation. Besides the issue of the boundary condition, to the authors' best knowledge, the current configuration has not been numerically studied before, so how to appropriately analyze the results and describe the flow characteristics using the known flow patterns to understand the new physical insights should be also taken into consideration.

Therefore, this study aims to investigate the unstable phenomena induced by the natural convection in a vertical channel with asymmetric hot-cold walls at moderate Rayleigh numbers from 5.2×10^5 to 7.6×10^6. To the authors' best knowledge, the physical model proposed here has not been studied yet due to the opposite directions of the velocity at the same boundary condition. To overcome this problem, the non-reflecting boundary condition with the absorbing boundary condition developed in [1] is applied to the current physical model. Besides, the unstable phenomena near the wall generate small flow structures, which is different from past cognitions about the flow pattern at the same Rayleigh number. To study the scale of the fluid property, following Ng et al. [2], the GL theory, originally proposed for the horizontal convection, is applied to investigate the flow and temperature fields to better understand the physics. Moreover, to further understand the mechanism of unstable phenomena, the effect of the Rayleigh number on the heat transfer is also investigated. From the result, it can be known that, even at a low Rayleigh number, once the interaction between hot and cold walls is strong enough, instead of the laminar flow field, the similar Rayleigh-Benard convection is shown and this kind of convection can enhance the heat transfer.

Physical model and Governing Euqation

The open-ended finite length channel with extra regions is shown in Fig. 1. The streamwise, vertical and spanwise directions are denoted x_1, x_2 and x_3, and their corresponding velocities are u_1, u_2 and u_3, respectively. Gravity is in the negative x_1 direction. For simplicity, only the x_1 x_2 plane is shown here as the boundary condition in the spanwise direction, x_3, is periodic. The channel has width l_2 and the origin is at point c. The whole computational domain can be separated to three parts, the real physical domain $abdc$, the lower artificial buffer zone a_0b_0ba, and the upper artificial buffer zone cdd_0c_0. The related parameters used in this study are listed in Table 1.

The real physical domain $abdc$ consists of the heat wall ac with an isothermal condition T_h and the cold wall bd with an isothermal condition T_c. The governing equations here are the original Navier–Stokes equations,

$$\frac{\partial U}{\partial t}+\frac{\partial F_1}{\partial x_1}+\frac{\partial F_2}{\partial x_2}+\frac{\partial F_3}{\partial x_3}=S\,. \tag{1}$$

i.e. compressible DNS. The quantities included in U and F_i are

$$U=\begin{pmatrix}\rho\\ \rho u_1\\ \rho u_2\\ \rho u_3\\ \rho e\end{pmatrix},\ F_i=\begin{pmatrix}\rho u_i\\ \rho u_i u_1+P\delta_{i1}-\mu A_{i1}\\ \rho u_i u_2+P\delta_{i2}-\mu A_{i2}\\ \rho u_i u_3+P\delta_{i3}-\mu A_{i3}\\ (\rho e+P)u_i-\mu A_{ij}u_j-k\partial T/\partial x_i\end{pmatrix},\quad S=\begin{pmatrix}0\\ -(\rho-\rho_0)g\\ 0\\ 0\\ -(\rho-\rho_0)gu_1\end{pmatrix}, \tag{2}$$

where $A_{ij}=\partial u_j/\partial x_i+\partial u_j/\partial x_i-2/3(\nabla\bullet u)\delta_{ij}$ and the ideal gas equation is written as $p=\rho RT$

The viscosity and thermal conductivity of the fluid are based upon Sutherland's law:

$$\mu(T) = \mu_0 (\frac{T}{T_0})^{\frac{3}{2}} \frac{T_0 + 110}{T + 110}, \quad (3)$$

$$k(T) = \frac{\mu(T)\gamma R}{(\gamma - 1)\Pr}, \quad (4)$$

Where $\rho_0 = 1.1842 kg/m^3$, $g = 9.8 m/s^2$, $\mu_0 = 1.85 \times 10^{-5} N \cdot s/m^2$, $T_0 = 298.0592 K$, $\gamma = 1.4$, $R = 287 J/kg/K$ and $\Pr = 0.72$.

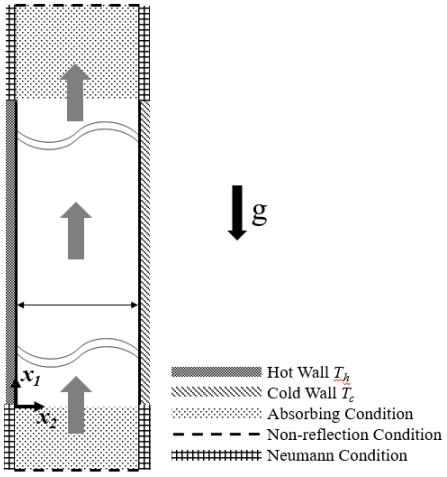

Figure 1. Physical Model

Owing to the buoyancy force generated by both the heat wall *ac* and cold wall *bd* that drives the fluid flow, it can be expected that the opposite direction of the velocity will be simultaneously existed on the *ab* and *cd*. This means that the edge a_0b_0 and c_0d_0 should be as far as possible from the domain of interest, *abcd*, to mimic the infinite environment. Therefore, the artificial buffer zones, a_0b_0ba and cdd_0c_0, are added to the real physical domain to reduce the computational requirements of mimicking the infinite environment.

$$\frac{\partial U}{\partial t} + \frac{\partial F_1}{\partial x_1} + \frac{\partial \xi}{\partial x_1} + \frac{\partial F_2}{\partial x_2} + \frac{\partial F_3}{\partial x_3} + \sigma = S, \quad (5)$$

where

$$\eta = \eta_1 \begin{pmatrix} \rho \\ \rho u_1 \\ \rho u_2 \\ \rho u_3 \\ \rho e \end{pmatrix}, \text{ and } \sigma = \sigma_1 \begin{pmatrix} \rho - \rho_{\text{target}} \\ \rho u_1 - (\rho u_1)_{\text{target}} \\ \rho u_2 - (\rho u_2)_{\text{target}} \\ \rho u_3 - (\rho u_3)_{\text{target}} \\ \rho e - (\rho e)_{\text{target}} \end{pmatrix}, \quad (6)$$

where ϕ_{target} is the target value at infinity. So, $\rho_{\text{target}} = 1.1842 kg/m^3$, $u_{i,\text{target}} = 0 m/s$ and $p_{\text{target}} = 101300 Pa$.

For the artificial buffer zones, the absorbing boundary condition is applied. Comparing with Eq. (1), the governing equations in artificial buffer zones have two additional terms; the artificial convection term, $\partial\xi/\partial x_1$, to drive the convection velocity to the desired velocity at a_0b_0 and c_0d_0, and the damping term, σ, to eliminate disturbances. Following Li et al. [1], for the artificial buffer zones a_0b_0ba, η_1 and σ_1 are expressed as

$$\xi_1 = V_{out} \times c' \times [(x_1 - \overline{ac}) / \overline{aa_0}]^3, \quad (7)$$

$$\sigma_1 = \sigma_{out} \times c' \times [(x_1 - \overline{ac}) / \overline{aa_0}]^3, \quad (8)$$

where V_{out} and σ_{out} are 1.25 and c' is calculated from Eq. (9).

$$c' = 0.5 \times \sqrt{u^2(\Theta - 1)^2 + 4\Theta c^2}, \quad (9)$$

where $\Theta \approx 100(U_0/c)^2$ and c is the speed of sound. Similarly, for the artificial buffer zones cdd_0c_0, η_1 and σ_1 are expressed as

$$\xi_1 = V_{in} \times c' \times (-x_1 / \overline{cc_0})^3, \quad (10)$$

$$\sigma_1 = \sigma_{out} \times c' \times (-x_1 / \overline{cc_0})^3, \quad (11)$$

however, σ_1 is set as 0.035 to not to excessively damp out the fluctuation when the flow enters the real physical domain.

In addition to the absorbing boundary condition, to prevent thermal diffusion from the edge of the arstificial buffer zone back into the domain, thereby polluting the results, the modified local one-dimensional inviscid (LODI) relations is applied at the edge of the artificial buffer zone as the non-reflecting boundary condition. For more detail information about the absorbing and non-reflecting boundary conditions mentioned above, Li et al. [1] can be referred.

Numerical Method

The fluid speed induced by the natural convection is nearly the incompressible flow so the original compressible solver should be modified for this study. The original Roe scheme with a preconditioning method and dual time stepping, which has been proved to be a powerful tool for the transient natural convection simulation in [3,4,5] is applied to resolve Eq. (1). Hence, the new governing equations employed to the curvilinear coordinates (ξ, η, ζ) to better resolve the near-wall physics is

$$\Gamma \frac{\partial \bar{U}_p}{\partial \tau} + \frac{\partial \bar{U}}{\partial t} + \frac{\partial \bar{F}_1}{\partial \xi} + \frac{\partial \bar{F}_2}{\partial \eta} + \frac{\partial \bar{F}_3}{\partial \zeta} = \bar{S}, \quad (9)$$

where Γ is the preconditioning matrix derived by Weiss and Smith [6], $\bar{U}_p$ is the primitive form of $[P, u_1, u_2, u_3, T]/J$ in which J is the Jacobian transformation matrix, τ and t are the artificial and physical times, respectively, and $\bar{U}$ is the conservative form of $(\rho, \rho u_1, \rho u_2, \rho u_3, \rho e)/J$. For $\bar{S}$, in the real physical domain, *abdc*, $\bar{S} = S/J$; in the artificial buffer zone, a_0b_0ba and cdd_0c_0, $\bar{S} = -(\partial\xi/\partial x_1 + \sigma)/J + S/J$.

The discretized form of Eq. (9) is

$$\begin{aligned} &\Gamma \frac{\bar{U}_p^{k+1} - \bar{U}_p^k}{\Delta\tau} + \frac{3\bar{U}^{k+1} - 4\bar{U}^n + \bar{U}^{n-1}}{2\Delta t} \\ &+ \frac{1}{\Delta\xi}(\bar{F}^{k+1}_{1_{i+\frac{1}{2},j,k}} - \bar{F}^{k+1}_{1_{i-\frac{1}{2},j,k}}) + \frac{1}{\Delta\eta}(\bar{F}^{k+1}_{2_{i,j+\frac{1}{2},k}} - \bar{F}^{k+1}_{2_{i,j-\frac{1}{2},k}}), \\ &+ \frac{1}{\Delta\zeta}(\bar{F}^{k+1}_{3_{i,j,k+\frac{1}{2}}} - \bar{F}^{k+1}_{3_{i,j,k-\frac{1}{2}}}) = \bar{S} \end{aligned} \quad (10)$$

The terms $\partial\bar{U}_p/\partial\tau$ and $\partial\bar{U}/\partial t$ are approximated by a first-order forward difference and a second-order backward difference, respectively, and the terms $\partial\bar{F}_1/\partial\xi$, $\partial\bar{F}_2/\partial\eta$, and $\partial\bar{F}_3/\partial\zeta$ are approximated by a central difference. The

superscripts k and n indicate the iteration numbers of artificial time and the proceeding step of real time, respectively. When the artificial time $\partial \bar{U}_p / \partial \tau$ converges to $\varepsilon(=10^{-2})$, the magnitude of the $(k+1)th$ iteration of the artificial time term is approximately equivalent to the magnitude of the $(n+1)th$ time step of the real time, reducing Eq. (10) to the original Navier–Stokes equation including the transient term.

Finally, Eq. (10) can be rearranged as

$$[\frac{I}{\Delta\tau}+\Gamma^{-1}M\frac{3}{2\Delta t}+ \Gamma^{-1}(\delta_\xi A_p^k+\delta_\eta B_p^k+\delta_\varsigma C_p^k)]\Delta U_p=\Gamma^{-1}R^k, \quad (11)$$

where $M=\partial \bar{U}_p/\partial\tau$, δ_ξ is the central-difference operator, $A_p=\partial \bar{F}_1^k/\partial \bar{U}_p$ is the flux Jacobian and $R^k=\bar{S}-(3\bar{U}^k-4\bar{U}^n+\bar{U}^{n-1})/2\Delta t-(\delta_\xi \bar{F}_1^k+\delta_\eta \bar{F}_2^k+\delta_\varsigma \bar{F}_3^k)$. Eq. (11) is solved using the Lower-Upper Symmetric-Gauss-Seidel (LUSGS) implicit method.

In the computation of R^k on the right-hand side of Eq. (11), the terms of F_i in Eq. (2) based on Cartesian coordinates can be divided into two parts. One is the inviscid term,

$$F_{inviscid}=\begin{pmatrix}\rho u_i\\ \rho u_i u_1+P\delta_{i1}\\ \rho u_i u_2+P\delta_{i2}\\ \rho u_i u_3+P\delta_{i3}\\ (\rho e+P)u_i\end{pmatrix}, \quad (12)$$

the other is the viscous term,

$$F_{viscous}=-\begin{pmatrix}0\\ \mu A_{i1}\\ \mu A_{i2}\\ \mu A_{i3}\\ \mu A_{ij}u_j+\lambda\dfrac{\partial T}{\partial x_i}\end{pmatrix}, \quad (13)$$

The Roe scheme is employed in the discretization of the $F_{inviscid}$ term and, when the preconditioning matrix is added, is expressed as

$$F_{inviscid,i+\frac{1}{2}}=\frac{1}{2}(F_R+F_L)-\frac{1}{2}\left\{\left|\Gamma^{-1}A_p\right|\Delta U_P\right\}, \quad (14)$$

For the reconstruction of F_R and F_L, the fifth-order monotonic upstream-centred scheme (MUSCL) without a limiter function to prevent turbulent fluctuations from attenuating, is adopted and expressed as

$$U_{L,i+1/2}=1/60\times(2U_{i-2}-13U_{i-1}+47U_i+27U_{i+1}-3U_{i+2}), \quad (15)$$

$$U_{R,i-1/2}=1/60\times(-3U_{i-2}+27U_{i-1}+47U_i-13U_{i+1}+2U_{i+2}), \quad (16)$$

Aside from the inviscid term, the derivative terms in A_{ij} are computed by a second-order central difference. For the artificial convection term, $\partial\xi/\partial x_1$, in Eq. (13), the first-order backward difference is used, which is expressed as

$$\frac{\Delta\xi}{\Delta x_1}=\frac{\xi_i-\xi_{i-1}}{\Delta x_1}=\xi_1\frac{U_i-U_{i-1}}{\Delta x_1}, \quad (17)$$

For the boundary condition, all walls are assumed to be isothermal and no-slip conditions. For a_0a, b_0b, cc_0 and dd_0 in the lateral direction, Neumann condition is adopted. In the x_3 direction, the periodic condition is also implemented to reduce the computational effort.

Result and Discussion

The natural convection in a vertical channel as shown in Fig. 1 is investigated and the Rayleigh number based on the width of the channel is 5.2×10^5. Two different cases are conducted. One is that the wall temperatures in the left and right are $T_c=T_0-20K$ and $T_h=T_0+40K$, respectively (CaseI). The other is that the wall temperatures in the left and right are $T_c=T_0$ and $T_h=T_0+60K$, respectively (CaseII). The detail computational parameters are listed in Table. 1. Please note here. The temperature differences between two walls for these two cases are the same so that the Rayleigh numbers are also identical.

Table. 1 Computational parameters

Δt	$2.0\times10^{-3}\ s$
Wall Temperature	CaseI: $T_c=T_0-20K$; $T_h=T_0+40K$ CaseII: $T_c=T_0$; $T_h=T_0+60K$
$\Delta T=T_h-T_c$	$60\ K$
H	$0.045\ m$
L	$0.4\ m$
Ra	5.2×10^5
$U_{\Delta T}$	$\sqrt{g\beta\Delta TH}=0.3$
Domain size	$0.65\times0.045\times0.02\ \ m^3$
$\Delta x_1\times\Delta x_2\times\Delta x_3$	$1\times0.1\times2\ \ mm^3$
$N_1\times N_2\times N_3$	400×200×100 (Physical domain)

Fig 2. shows the contour of the instantaneous temperature and the instantaneous velocity for both CaseI and CaseII. For the CaseII, except the region near the outlet, the flow field and the temperature field are almost stationary. On the other hand, CaseI shows unstable phenomena. Generally speaking, at this moderate Rayleigh, the natural convection in a vertical channel should be stationary such as shown in CaseII. Therefore, it can be known that the existing empirical experience for the vertical channel flow can't be applied to Case I.

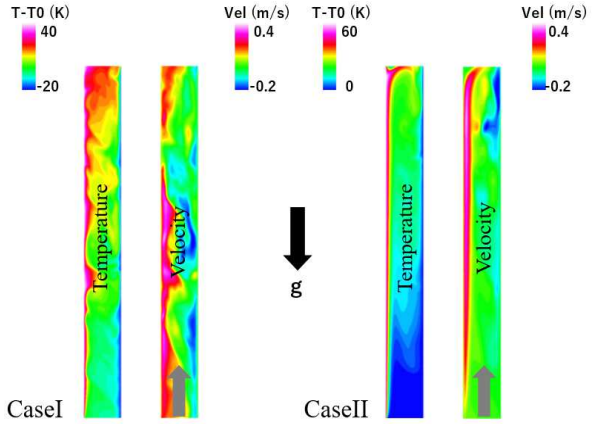

Figure 2. The instantaneous temperature and velocity contour

To investigate the unstable phenomena in CaseI, the statistical data of the natural convection in a vertical channel but with periodic conditions in both spanwise and streamwise directions at the similar Ra number, 5.4×10^5, in [2] using DNS is compared in Fig. 3. Please note here. The discrepancy especially near the center of the channel height, $x_2/H=0.5$, is caused by the different conditions of the temperature on the wall. In [2], the condition of $T_H=T_0+1/2\times\Delta T$ and $T_c=T_0-1/2\times\Delta T$ is assigned. On the other hand, in CaseI, the condition of $T_H=T_0+2/3\times\Delta T$ and $T_c=T_0-1/3\times\Delta T$ is assigned. The asymmetric distribution indicates that although the results are qualitatively good agreement with the DNS results, the current boundary condition can count the effect from the ambient condition that the periodic condition adopted in [2] couldn't. Besides, it can be also confirmed that the unstable phenomena here can be maintained to generate the turbulent structures near the wall.

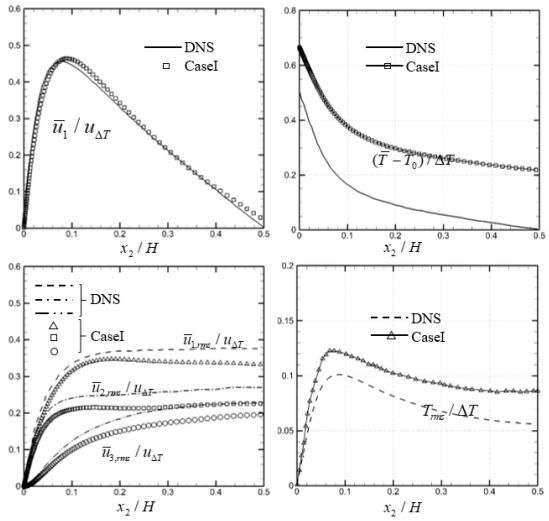

Figure 3. Statistical data

To study the flow and thermal fields near the wall, the boundary-layer behavior is investigated. Following [2], for the hot wall, the kinetic boundary-layer thickness δ_u is calculated by intercepting $\overline{u}=x_2\times d\overline{u}/dx_2$ and $\overline{u}=\overline{u}_{\max}$. Similarly, the thermal boundary-layer thickness δ_T is calculated by intercepting $\overline{T}=T_h+x_2\times d\overline{T}/dx_2$ and $\overline{T}=T_h-2/3\times\Delta T$. Through these calculations, the effects on the flow can be separated. One is from the boundary layer due to the velocity gradient, $d\overline{u}/dx_2$ (Inside the BL) and the other is from the bulk region caused by the bulk velocity, $\overline{u}=\overline{u}_{\max}$ (Outside the BL). These distributions are compared with the kinetic dissipation and the thermal dissipation in Fig. 4. to better understand the physical insight. The kinetic dissipation due to the mean velocity, $\overline{\varepsilon}_{\overline{u}}=\mu(\mathrm{d}\overline{u}_2/\mathrm{d}x_2)$ and due to the velocity fluctuations $\overline{\varepsilon}_{u'}=\overline{\mu(\partial u_i'/\partial x_j)^2}$, and the thermal dissipation due to the mean temperature, $\overline{\varepsilon}_{\overline{T}}=k(\mathrm{d}\overline{T}/\mathrm{d}x_2)$ and due to the temperature fluctuations, $\overline{\varepsilon}_{T'}=k\overline{(\partial T'/\partial x_j)^2}$ are shown. Based on these results, inside the boundary layer, the physical properties of the mean dominate the flow field. On the other hand, outside the boundary layer, the physical properties of the fluctuation dominate the flow field. The flow field shows both laminar and turbulent behaviors, which is consistent with the GL theory, therefore, can be explained as follows: because away from the wall, the turbulence due to the natural convection is not strong enough to generate the boundary layer, the kinetic dissipation is eventually decomposed into the laminar behavior inside the boundary layer and turbulent behavior outside the boundary layer.

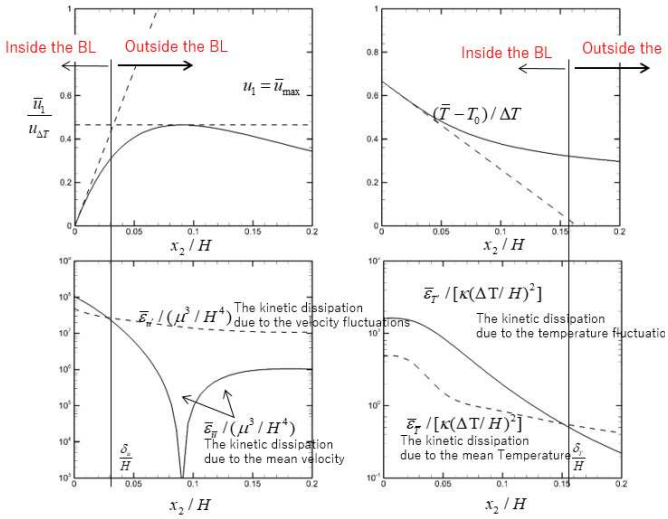

Figure 4. The distribution of the kinematic dissipation and the thermal dissipation

The correlation between the Rayleigh number and Nusselt number at the half-length of the channel, $x_1=0.2m$, is shown in Fig. 5. The distribution shows a discontinuous trend between $Ra=4.0\times10^6$ and $Ra=6.0\times10^6$. Different from the rest of the other distribution, with increasing the Rayleigh number, the increment of the Nusselt number can't be observed during this range. Based on the results of $Ra=4.19\times10^6$ and $Ra=5.74\times10^6$ shown in Fig. 5, the reason that the Nu is not increased can be blamed on the lack of these unstable phenomena. At $Ra=4.19\times10^6$, the interaction of the heat transfer between two walls is disappeared so the effect of enhancing the heat transfer from this instability does not exist anymore. Hence, the trend of the increment of the Nusselt numbers can't be maintained when Ra is larger than 4.19×10^6. Moreover, by extending the distribution of $Ra<4.19\times10^6$, the differences of the distribution between $Ra<4.19\times10^6$ and $Ra>5.74\times10^6$ can be seen as the effect of the unstable phenomena, which can be estimated around 10%. In other words, the unstable phenomena will increase the performance of the heat transfer by around 10%.

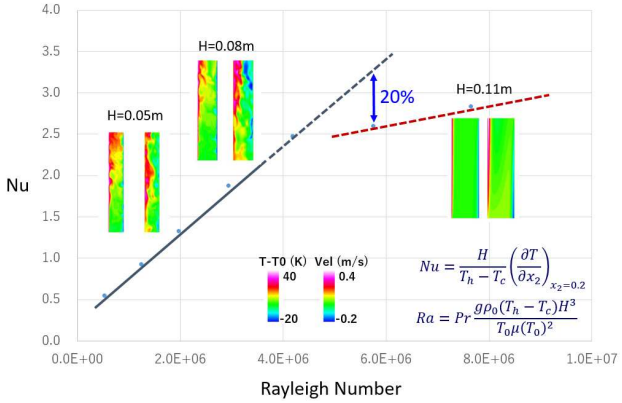

Figure 5. The correlation between Ra and Nu

Conclusion

The natural convection in an open-ended vertical channel with a hot-cold wall configuration has been studied for the first time. The compressible solver with the hybrid boundary condition is utilized to address the problem of the unknown flow rate at the inlet and outlet. Based on the statistical data, it can be known that the existing empirical experience for the vertical channel flow cannot be applied to the present study. Instead, it is found that GL theory, originally proposed for horizontal convection, can well describe the unstable phenomena here. From the result of the Rayleigh-Nusselt number correlation, it can be known that the unstable phenomena due to the interaction between two walls can enhance the heat transfer by around 10%.

REFERENCES

[1] C.-G. Li, M. Tsubokura, W.-S. Fu, N. Jansson, W.-H. Wang, Compressible direct numerical simulation with a hybrid boundary condition of transitional phenomena in natural convection, Int. J. Heat Mass Transf. 90 (2015).

[2] C.S. Ng, A. Ooi, D. Lohse, D. Chung, Vertical natural convection: Application of the unifying theory of thermal convection, J. Fluid Mech. 764 (2015) 349–361.

[3] W.-S. Fu, C.-G. Li, C.-C. Tseng, An investigation of a dual-reflection phenomenon of a natural convection in a three dimensional horizontal channel without Boussinesq assumption, Int. J. Heat Mass Transf. 53 (2010) 1575–1585.

[4] C.G. Li, M. Tsubokura, W.S. Fu, N. Jansson, W.H. Wang, Compressible direct numerical simulation with a hybrid boundary condition of transitional phenomena in natural convection, Int. J. Heat Mass Transf. 90 (2015) 654–664.

[5] C.G. Li, A compressible solver for the laminar–turbulent transition in natural convection with high temperature differences using implicit large eddy simulation, Int. Commun. Heat Mass Transf. 117 (2020).

[6] J.M. Weiss, W.A. Smith, Preconditioning applied to variable and constant density flows, AIAA J. 33